Introducing F-Scan to the Concurrent Imaging Mode

João Pedro Turchetti Ribeiro[*,**], **Thomas Kraus**[*], **Markus Bachmann**[*], **Renato Machado**[**]

[*]German Aerospace Center (DLR)
Oberpfaffenhofen, Germany
email: joao.turchettiribeiro@dlr.de

[**]Aeronautics Institute of Technology (ITA)
São José dos Campos, Brazil
email: rmachado@ita.br

Abstract: *The concurrent imaging mode is a recently proposed technique to increase the imaging capability and flexibility of SAR systems. It allows for simultaneous acquisitions of two areas by increasing the pulse repetition frequency (PRF) and interleaving the transmission and the reception of two modes in a pulse-to-pulse manner. Due to intrinsic system limitations, this technique applied to current operational systems, such as the German SAR satellite TerraSAR-X, comes along with strong trade-offs in terms of limited swath width and increased ambiguity levels. For future X-band missions, the frequency scanning (F-Scan) technique is one of the most promising methods to improve these performance parameters. Therefore, this paper derives timing and interference analyses for the integration of F-Scan with the concurrent imaging concept. Additionally, it will be shown that F-Scan can improve the main critical performance parameters of the concurrent mode.*

1. Introduction

Synthetic aperture radar (SAR) systems can operate with different imaging modes depending on the specific application. For instance, the Staring Spotlight can be used to image a small area on ground with a very high resolution [1], [2]. Conversely, the ScanSAR mode acquires larger scenes, but at the expense of a coarser resolution. Finally, the well-known Stripmap mode achieves a more balanced performance, with medium coverage and medium resolution [3], [4].

One of the limitations of the current state-of-the-art imaging modes is that only one can be used at a time. Due to the satellite's orbit geometry, there is a relatively long interval for low Earth orbits (LEO) between consecutive flyovers of the system over a given target on Earth under the same geometry, also known as the repeat cycle. In the TerraSAR-X case, this period is of 11 days. If two different acquisitions are required in nearby regions, then it may be necessary to wait up to this long. Generally speaking, any two nearby sites of interest, primarily separated in the range direction, could be required in specific applications. For instance, one could think of a requirement of imaging with the highest possible resolution (mode) the cities of Rio de Janeiro and São Paulo, or London and Amsterdam, which are roughly 350 km apart. The regions could

978-3-944976-34-1

also be in the same area, for instance, if a Stripmap image is required over a city and a Staring Spotlight image is simultaneously desired over the airport area.

One possible solution is to deploy a constellation of satellites at different orbit positions so that there is a shorter interval between the acquisitions [5]. However, this solution can be expensive and only shortens the revisit time, but does not eliminate it. To overcome this restriction, a concurrent imaging mode was introduced in [6], and further detailed in [7–9]. The idea of the proposed concurrent technique is to interleave two imaging modes (e.g. Stripmap and Stripmap, or Stripmap and Spotlight) in a pulse-to-pulse manner, so that two images are simultaneously acquired. It was shown that this technique indeed achieves increased flexibility and improved imaging capability. Nevertheless, trade-offs are necessary to achieve such improvements. Namely, ambiguities and swath width were demonstrated to be critical parameters for concurrent acquisitions.

Currently in the literature many references can be found proposing improvements to SAR systems by the means of digital beamforming (DBF) [10–12]. However, DBF systems are complex and hard to realize within restricted budgetary constraints. For X-band systems, a cost-effective alternative for DBF was proposed for the use of upcoming missions [13]. Taking advantage of the new ITU allocation allowing for a transmit bandwidth of 1200 MHz in X-band, the frequency scanning (F-Scan) technique was introduced in [14–16]. It consists of an analog beamforming technique to achieve steering in elevation that can be implemented with much less hardware complexity than DBF. Besides being more affordable, F-Scan also brings primary improvements in terms of signal-to-noise ratio (SNR), impulse response and reduced peak power requirement.

The paper is structured as follows. In Section 2, the imaging concept of F-Scan is explained in more details, followed by timing considerations. Next, in Section 3, the concurrent imaging aspects are described and merged with the F-Scan timing analysis. Additionally, the timing interferences are assessed and visualized. Section 4 presents a first assessment of the performance improvements of the concurrent mode that can be achieved by the F-Scan system. Finally, concluding remarks are given in Section 5.

2. F-Scan Concepts and Timing Analysis

In conventional Stripmap acquisitions, a fixed wide beam in elevation is used both on transmission and on reception. F-Scan, in contrast, transmits and receives with a sweeping high-gain pencil beam. The used waveform is a linear frequency modulated (LFM) signal called chirp. The frequency variation is accompanied by sweeping the elevation beam over the target area from far to near range. The scan is achieved via analog beamforming, i.e., by using true time delay lines and phase shifters each frequency is associated with one elevation angle. The antenna system is designed such that a linear frequency variation leads to a roughly linear scanning of the antenna pattern. For instance, using an up-chirp, the lowest frequency of the chirp is transmitted towards the far edge of the scene, while the highest frequency is transmitted towards

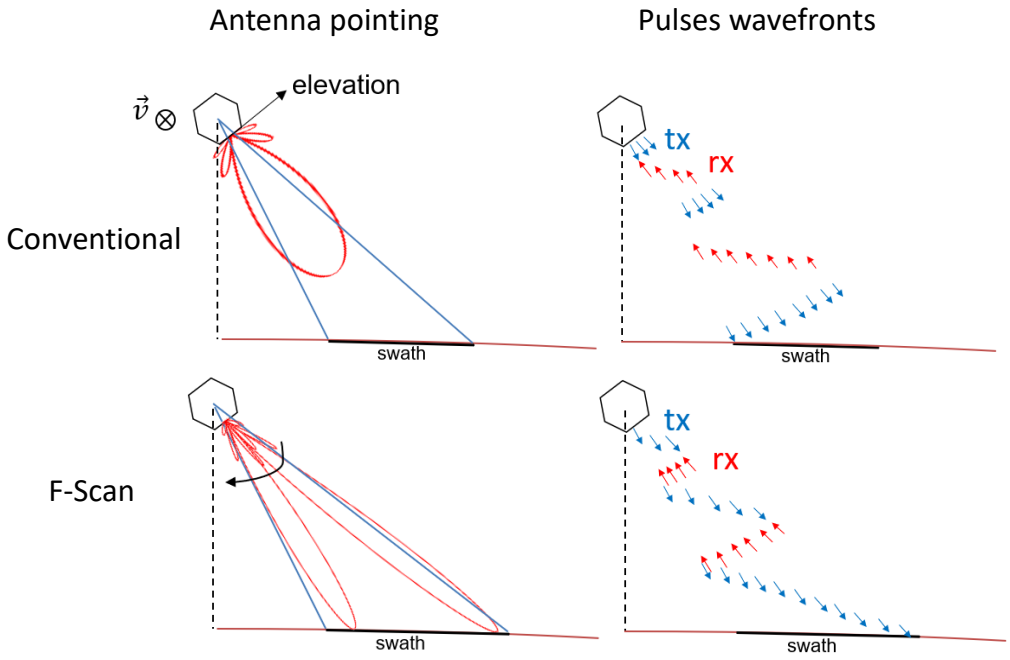

Figure 1: Schematic comparison of conventional Stripmap mode with F-Scan acquisitions. Conventional Stripmap employs a broad beam and receives first from near range. F-Scan, conversely, sweeps across the ground range with a pencil beam by linearly increasing the chirp frequency. As a result, the echoes overlap on receive.

the near edge. This mechanism and its comparison with the conventional Stripmap mode are schematically represented in Fig. 1.

In F-Scan, each target within the scene is considered fully imaged only if it is swept over by the whole half-power beamwidth (HPBW) region of the main lobe of the antenna pattern. Therefore, the antenna starts and finishes the transmission pointing outside the imaged area so as to ensure that the near and far edges are fully imaged. Geometrically, as depicted in Fig. 2, the antenna starts pointing towards a look angle β_f, while the effective furthest point of the scene is only at $\beta_\mathrm{f,eff} = \beta_\mathrm{f} - \frac{\mathrm{HPBW_{el}}}{2}$, with $\mathrm{HPBW_{el}}$ as the HPBW in elevation of the antenna. Similarly, the transmission ends at β_n, and the nearest point inside the scene is at $\beta_\mathrm{n,eff} = \beta_\mathrm{n} + \frac{\mathrm{HPBW_{el}}}{2}$. Considering the center frequency as f_c, the total transmit bandwidth B_t and a pulse duration of τ_p, Fig. 2 depicts the F-Scan transmit scheme in terms of time, frequency, and look angle.

An important factor of the F-Scan transmission is the illumination time of individual point targets within the scene, defined as dwell time in [17]. This parameter is calculated by

$$\tau_\mathrm{dwell} = \frac{\mathrm{HPBW_{el}}}{\beta_\mathrm{f} - \beta_\mathrm{n}} \cdot \tau_\mathrm{p}. \tag{1}$$

For a fixed transmit pulse duration, longer dwell times – either due to shorter scenes or wider beams – result in each point-target being imaged with a higher portion of the total bandwidth,

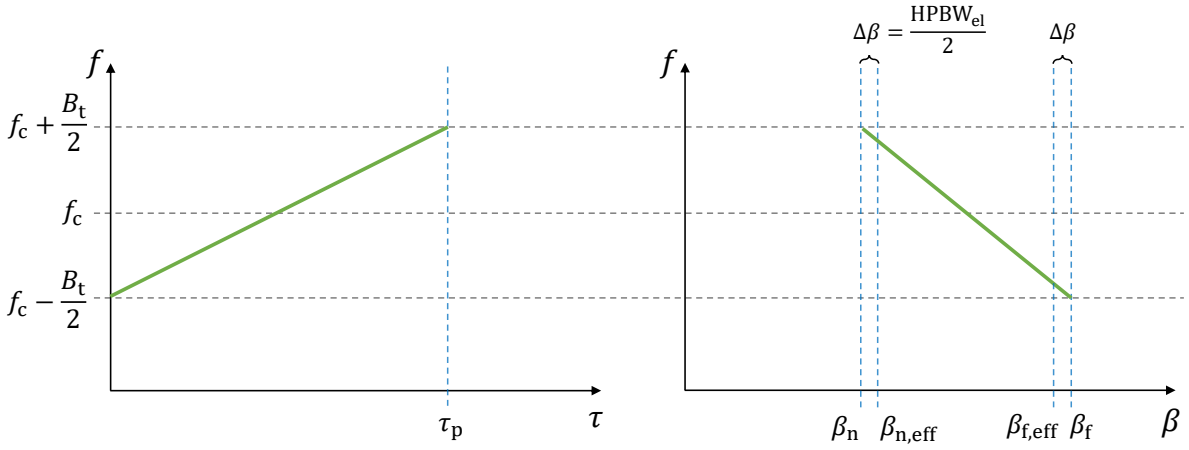

Figure 2: F-Scan instantaneous transmit frequency in terms of fast time (left) and look angle pointing of the peak of the main lobe (right).

thus increasing the range resolution. It can be then straightforwardly derived that the antenna starts transmitting with its leading edge towards the near range at the instant $\tau_{\mathrm{p}} - \tau_{\mathrm{dwell}}$. Consequently, a target at a look angle β starts to be imaged by the leading edge of the antenna at the instant τ_{lead} given by

$$\tau_{\mathrm{lead}}(\beta) = \frac{\beta_{\mathrm{f,eff}} - \beta}{\beta_{\mathrm{f,eff}} - \beta_{\mathrm{n,eff}}} \cdot (\tau_{\mathrm{p}} - \tau_{\mathrm{dwell}}) \;\; \forall\, \beta \in [\beta_{\mathrm{n,eff}}, \beta_{\mathrm{f,eff}}]. \tag{2}$$

For the timing of the echoes to be completely described, only the echo delay is missing. In other words, a relation between the look angle and the slant range must be defined. For simplicity, assuming a spherical model for the Earth's surface, the slant range can be calculated for the aforementioned look angle interval by

$$R(\beta) = \frac{\sin\left\{\sin^{-1}\left[\left(1 + \frac{H}{R_{\mathrm{E}}}\right) \cdot \sin\beta\right] - \beta\right\}}{\sin\beta} \cdot R_{\mathrm{E}}, \tag{3}$$

where R_{E} is the Earth's radius and H the satellite height.

Finally, with the echo delay given by $\tau_{\mathrm{delay}}(\beta) = 2R(\beta)/c$, and assuming the instant $\tau = 0$ to represent the beginning of the transmission, the antenna starts to receive echoes from targets at a look angle β at the instant $\tau_{\mathrm{rx,arrival}}(\beta) = \tau_{\mathrm{lead}}(\beta) + \tau_{\mathrm{delay}}(\beta)$. Naturally, the antenna stops receiving echoes from each target after a time equivalent to the illumination time (τ_{dwell}).

As frequency is an inherent aspect of the F-Scan, instead of the typical time by amplitude timing analysis, such acquisitions are better analyzed in the time by frequency domain. The timing analysis for F-Scan is summarized in Fig. 3 for an exemplary acquisition. The figure shows the instant and the frequencies of the received echoes from an extended target. The area in gray represents the echoes received with sufficient power, i.e., within the HPBW of the antenna pattern.

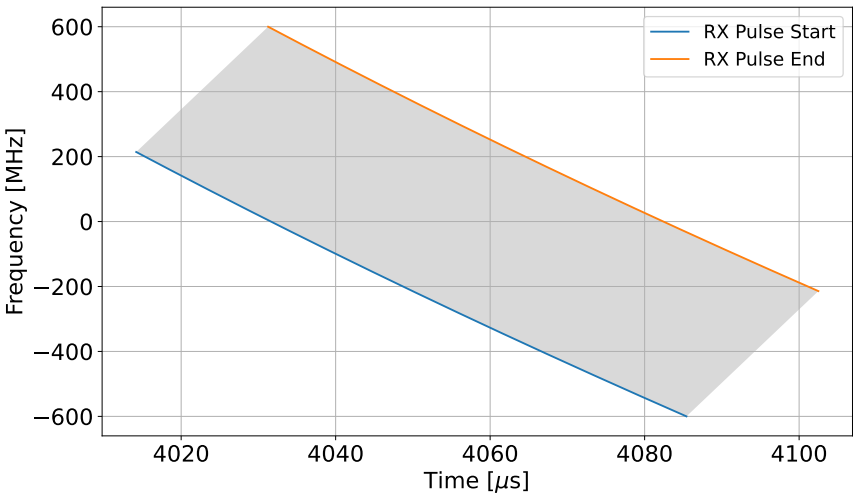

Figure 3: Schematic representation of the received F-Scan echoes in the time by frequency domain. The scene in question is at an incidence angle of 31.50°, and has a swath width of 30 km. The transmit pulse duration is 53 μs. The echo depicted is the first received, so that the x-axis represents the round trip delay.

Similarly, the arrival of the echoes depicted by the blue line can be seen as being originated by the leading edge of the pattern, while the orange line by the lagging edge. Such visualization is key in the determination of a proper pulse repetition frequency (PRF) for concurrent F-Scan acquisitions, as will be discussed in the following section.

3. Interference Assessment for Concurrent Imaging with F-Scan

Concurrent acquisitions as developed in [7] and [8] benefit from having extra degrees of freedom originated from the simultaneous imaging of two scenes. The interleaving of the modes in a pulse-to-pulse manner allows for the use of different pulse durations, duty cycles and incidence angles for each target area. The extra parameters introduce flexibility into the system, but at the same time the design of such a mode requires the determination of twice the amount of variables.

Additionally, the design of an F-Scan acquisition by itself is not as straightforward as of conventional SAR acquisitions. Due to the interrelation between the design parameters, such as pulse duration, swath width and required echo window, a graphical visualization through a traditional timing/diamond diagram is unfortunately not possible.

The approach taken in this paper for the PRF determination of concurrent acquisitions with F-Scan is to first determine the regions of interest, namely the scene sizes and the incidence angles, and also the required duty cycles, which are tightly related to the SNR. Then, the pulse duration for each mode can be investigated so as to achieve an interference-free scenario, i.e., free of transmit and Nadir interference.

On the one hand, transmit interference occurs when the antenna receives while it is transmitting. It must be avoided due to the high difference in power between the transmit signal and the received echoes. In monostatic systems, this power difference would saturate the receiver, not enabling the retrieval of the echoes.

Nadir interference, on the other hand, occurs when echoes coming from the ground straight below the satellite are received together with the echoes from the imaged scene. It leads to a bright line in the final focused image, strongly disturbing its quality [18], [19]. For concurrent acquisitions, however, an important distinction must be made relative to the Nadir echoes. Due to the independence in design between the transmit pulses of the modes, different waveforms, pulse durations and even bandwidths can be used. Therefore, same-mode Nadir interference must be differentiated from cross-mode Nadir interference. The latter represents the situation when the Nadir echoes originated from the transmit pulse of one mode is received during the echo window of the other mode.

To exemplify, from a timing perspective, a concurrent F-Scan acquisition with cross-mode Nadir interference, Fig. 4 schematically depicts the time by frequency transmit and receive events. In this example two 30 km Stripmap scenes are being imaged with toggling up and down chirps, one at the near range incidence angle of 31.50° and the other at 54.57°. The targets are 330 km apart. Moreover, different mode pulse repetition intervals (PRIs) and duty cycles are considered: 177 μs PRI with 30% duty cycle and 217 μs with 15%. In the figure, cross-mode Nadir interference in the reception of both modes can be clearly seen from the overlap between the Nadir and the Rx echoes. Such interferences have an opposite chirp rate than the simultaneously received echoes, so that they are not properly focused, thus not significantly disturbing the image quality. Additionally, due to recently published results showing the feasibility of removing the Nadir interference by a dual-focus approach with waveform diversity [20], one can assume the cross-mode Nadir interference to be tolerable from a timing perspective.

In concurrent acquisitions, it is important to highlight the difference between the PRI of each concurrently acquired mode and the effective PRI. The PRI of each mode is the total duration used for the mode's transmission followed by the reception. The effective PRI, in turn, is the azimuth sampling interval, i.e., how long it takes between consecutive receptions of the same mode. This is the value responsible for defining the azimuth resolution and the azimuth ambiguity ratio. For the previous example of two Stripmap images, the effective PRI can be obtained by

$$\mathrm{PRI}_{\mathrm{eff}} = \mathrm{PRI}^{\mathrm{SM1}} + \mathrm{PRI}^{\mathrm{SM2}}. \tag{4}$$

Similarly, one can also define the mode and the effective PRFs as the inverse of the respective PRIs.

For a combination of mode PRIs, Fig. 4 can be used to determine the interferences expected in the imaging. This assessment can be performed for a collection of PRIs and plotted in a

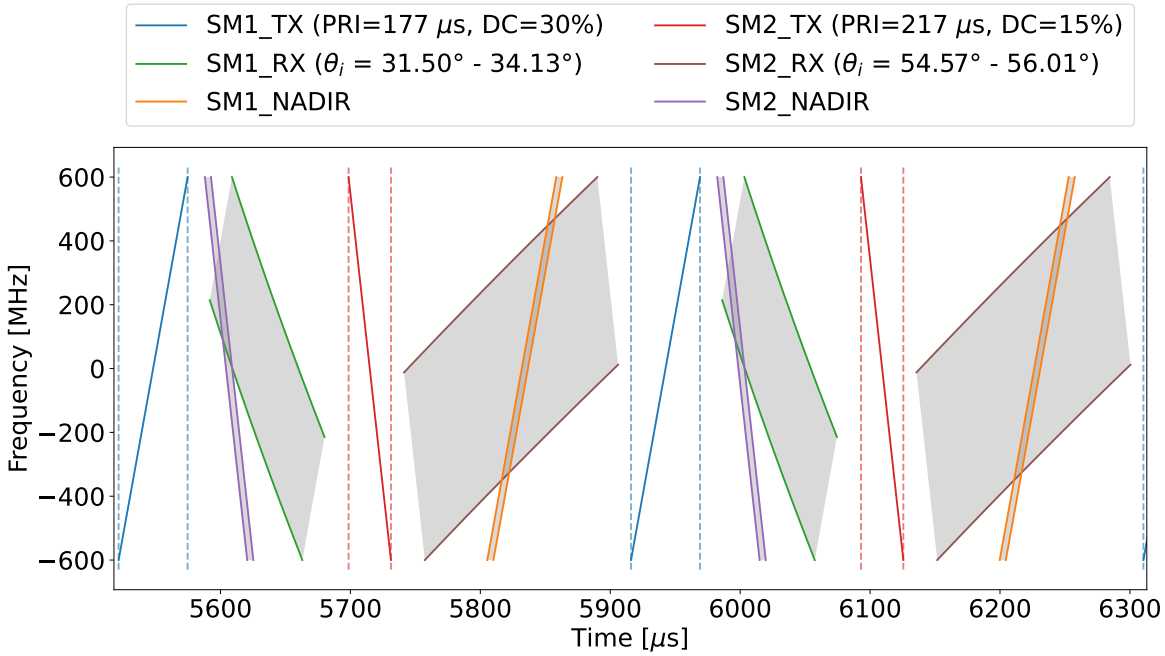

Figure 4: Schematic frequency representation of the transmit, receive and Nadir events of an F-Scan concurrent acquisition over time. The instant zero represents the transmission of the first pulse, and the depicted time interval was chosen based on the reception of the first echoes from the farther scene.

two-dimensional interference map. For the scenario previously considered, with near ranges at incidence angles of 31.50° and 54.57°, coupled with duty cycles of 30% and 15%, Fig. 5 shows the interference maps for concurrent F-Scan acquisitions with two 20 km and two 30 km wide swaths on the left and on the right side, respectively.

The interference maps have the mode PRIs on their axes, or, considering the duty cycles, the transmit pulse durations. The maps depict not only the interferences but also other timing restrictions. For instance, if the individual mode PRIs are too high – low effective PRF –, then the azimuth spectrum is aliased, and azimuth ambiguities occur. Here the threshold was set to a minimum effective PRF of 2000 Hz. This restricted area is highlighted in dark gray on the map. On the other hand, if the PRIs are too low, the echo windows are too short to fit the echoes from the scene. This effect is depicted in light gray on the interference maps. This area is larger for the 30 km scenario, as the wider scenes require larger echo windows.

It is important to note that a single PRI combination – either free of interferences or with only cross-mode Nadir interference – is sufficient to allow for an acquisition. So, even though the pink and white areas are clearly limited and small, the presence of only one combination is already enough from a timing perspective. Naturally, allowing for shorter swath widths brings more flexibility in the PRF selection.

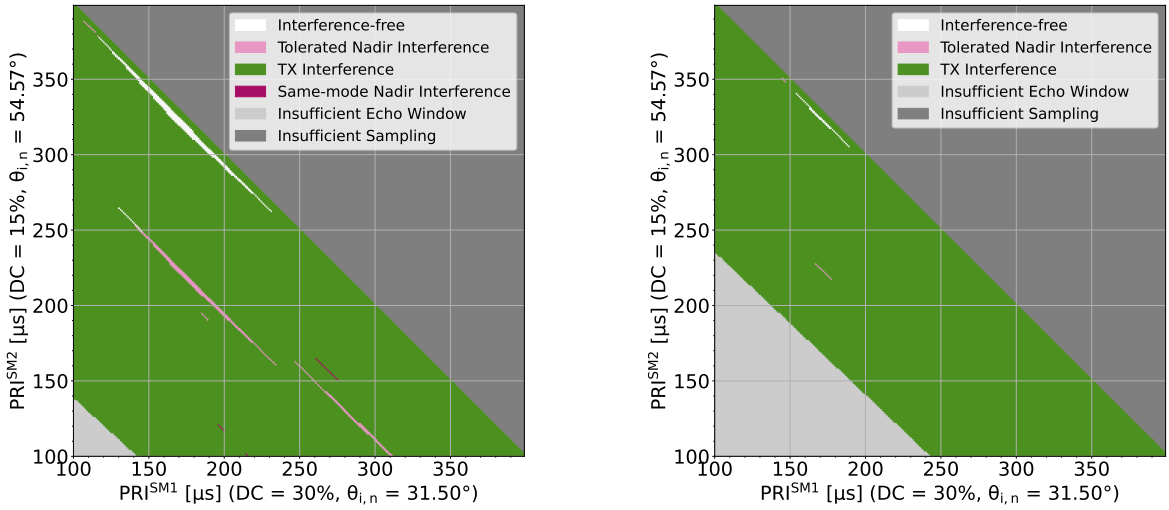

(a) Two 20 km scenes.

(b) Two 30 km scenes.

Figure 5: Interference maps for concurrent acquisitions with F-Scan portraying the available PRI combinations and the interference events. The allowed areas are indicated by the white and pink colors. On the left, two scenes with 20 km of swath width are considered, while, on the right, the swath widths are increased to 30 km.

4. Mission Application

The procedure to determine the PRFs for a concurrent F-Scan acquisition was previously described. So as to visualize the actual improvements brought by the F-Scan technique, two systems are compared in this section. On the one hand, the concurrent imaging capability of TerraSAR-X (TSX) is taken as the state-of-the-art benchmark [8]. On the other hand, the proposed HRWS system, with its bigger antenna and F-Scan capability, is considered [21], [22]. A first assessment of the average performance improvement achieved by the new system is summarized in Table 1.

The most significant achievement of F-Scan is the simultaneous improvement of the scene size and the resolution. Due to its better time domain efficiency, the F-Scan manages to increase the swath width by about 50%. With the help of the higher bandwidth, the two-dimensional resolution is also improved by a factor of roughly three to four. The SNR is not expected to be significantly degraded due to the use of a high bandwidth, as high gain pencil beams are used both on transmission and reception. In case a larger antenna aperture were considered, SNR and range ambiguity performance would be further improved, but at the expense of lower range resolution and higher hardware costs. Finally, the maximum distance between the targets is also extended from 250 km to 350 km. This extension is achieved by the better range ambiguity and SNR performance obtained by the F-Scan. In other words, targets at higher incidence angles can now be imaged without relevant image degradation.

Table 1: Summary of the performance improvements of the concurrent imaging technique achieved with F-Scan in comparison to with the traditional Stripmap mode.

	Traditional SM (TSX)	**F-Scan (HRWS)**
Antenna size	0.7 m (El.) / 4.8 m (Az.)	1.4 m (El.) / 6.0 m (Az.)
Bandwidth	100 MHz	1200 MHz
Swath width	2x 20 km	2x 30 km
Distance (swaths)	80 - 250 km	80 - 350 km
Resolution (θ_i = 25°)	12.8 m^2	4.6 m^2
Resolution (θ_i = 45°)	7.6 m^2	1.8 m^2

5. Conclusion

The concurrent imaging mode has the benefit of simultaneously acquiring two SAR images, discarding the need to wait for the next flyover. In order to tackle the main challenges of concurrent imaging, namely ambiguities and swath width, the F-Scan technique can be considered. This paper addresses in detail the procedures to design a concurrent F-Scan acquisition from a timing perspective. The F-Scan characteristics are initially described, followed by its integration with the concurrent imaging aspects. Considering the proposed German X-band mission HRWS, the F-Scan was shown to extend the range of use of the concurrent imaging mode by obtaining wider, farther apart, and higher resolution scenes. The excellent results highlight improvements achieved by combining F-Scan with the concurrent technique, paving the way for further investigation.

References

[1] W. G. Carrara, R. S. Goodman, and R. M. Majewski, *Spotlight Synthetic Aperture Radar*. Norwood, MA: Artech House, 1995.

[2] J. Mittermayer, S. Wollstadt, P. Prats-Iraola, and R. Scheiber, "The TerraSAR-X staring spotlight mode concept," *IEEE Transactions on Geoscience and Remote Sensing*, vol. 52, pp. 3695–3706, 2014.

[3] J. Curlander and R. McDonough, *Synthetic Aperture Radar: Systems and Signal Processing*. New York: Wiley, 1991.

[4] I. G. Cumming and F. H. Wong, *Digital Signal Processing of Synthetic Aperture Radar Data: Algorithms and Implementation*. Norwood, MA: Artech House, 2005.

[5] S. Suri, L. Peterson, A. Kaptein, F. Cerezo, V. Moreno, and M. A. G. Primo, "TerraSAR-X/PAZ constellation: CONOPS, highlights and access solution," in *Proc. APSAR*. Singapore: IEEE, 2015, pp. 178–183.

[6] D. Calabrese, V. Mastroddi, S. Federici, and S. Serva, "Discrete stepped strip (DI2S) for multi-swath acquisitions," in *IEEE 5th Asia-Pacific Conference on Synthetic Aperture Radar (APSAR)*. Singapore: IEEE, 2015, pp. 191–195.

[7] T. Kraus, J. P. T. Ribeiro, M. Bachmann, U. Steinbrecher, and C. Grigorov, "Concurrent imaging for TerraSAR-X: Wide-area imaging paired with high-resolution capabilities," *IEEE Transactions on Geoscience and Remote Sensing*, vol. 60, pp. 1–14, 2022.

[8] J. P. T. Ribeiro, T. Kraus, M. Bachmann, and R. Machado, "Multiple PRI technique for concurrent imaging mode using TerraSAR-X," in *Proc. IEEE Radar Conference*. New York City, NY, USA: IEEE, 2022, pp. 1–6.

[9] T. Kraus, J. P. T. Ribeiro, M. Bachmann, and R. Machado, "Ambiguity assessment and mitigation approaches for the TerraSAR-X concurrent imaging technique," in *Proc. EUSAR*. Leipzig, Germany: VDE, 2022, pp. 1–6.

[10] M. Younis, C. Fischer, and W. Wiesbeck, "Digital beamforming in SAR systems," *IEEE Transactions on Geoscience and Remote Sensing*, vol. 41, pp. 1735–1739, 2003.

[11] G. Krieger, N. Gebert, and A. Moreira, "Multidimensional waveform encoding: A new digital beamforming technique for synthetic aperture radar remote sensing," *IEEE Transactions on Geoscience and Remote Sensing*, vol. 46, pp. 31–46, 2008.

[12] A. Moreira, G. Krieger, I. Hajnsek, K. Papathanassiou, M. Younis, P. Lopez-Dekker, S. Huber, M. Villano, M. Pardini, M. Eineder, F. D. Zan, and A. Parizzi, "Tandem-L: A highly innovative bistatic SAR mission for global observation of dynamic processes on the Earth's surface," *IEEE Geoscience and Remote Sensing Magazine*, vol. 3, pp. 8–23, 2015.

[13] A. Moreira, M. Zink, M. Bartusch, A. E. N. Quiroz, and S. Stettner, "German spaceborne SAR missions," in *Proc. 2021 IEEE Radar Conference*. Atlanta, GA, USA: IEEE, 2021, pp. 1–6.

[14] C. Roemer, "Introduction to a new wide area SAR mode using the F-Scan principle," in *Proc. IEEE Geosci. Remote Sens. Symp. (IGARSS)*. Fort Worth, TX, USA: IEEE, 2017, pp. 3844–3847.

[15] C. Roemer, R. Gierlich, J. Marquez-Martinez, and M. Notter, "Frequency scanning applied to wide area SAR imaging," in *Proc. EUSAR*. Aachen, Germany: VDE, 2018, pp. 1–5.

[16] C. Roemer, "High resolution wide swath synthetic aperture system," International Patent WO 2019/015 911 A1, 2019.

[17] M. Younis, F. Q. de Almeida, T. Bollian, M. Villano, G. Krieger, and A. Moreira, "A synthetic aperture radar imaging mode utilizing frequency scan for time-of-echo compression," *IEEE Transactions on Geoscience and Remote Sensing*, vol. 60, pp. 1–17, 2022.

[18] S. Wollstadt and J. Mittermayer, "Nadir margins in TerraSAR-X timing commanding," in *Proceedings of the Committee on Earth Observation Satellites (CEOS)*, 2008, p. 4.

[19] J. Balkoski and F. Bordoni, "Nadir echo properties, a study based on TerraSAR-X data," in *Proc. 20th Telecommunications Forum (TELFOR)*, 2012.

[20] M. Villano, G. Krieger, and A. Moreira, "Nadir echo removal in synthetic aperture radar via waveform diversity and dual-focus postprocessing," *IEEE Geoscience and Remote Sensing Letters*, vol. 15, no. 5, pp. 719–723, 2018.

[21] M. Bartusch, C. Bruens, A. E. Nuncio Quiroz, and S. Stettner, "HRWS: the upcoming german X-Band spaceborne SAR mission," in *Proc. EUSAR*. Berlin: VDE, 2021, pp. 1–4, online event.

[22] J. Mittermayer, G. Krieger, A. Bojarski, M. Zonno, M. Villano, M. Pinheiro, M. Bachmann, S. Buckreuss, and A. Moreira, "MirrorSAR: An HRWS add-on for single-pass multi-baseline SAR interferometry," *IEEE Transactions on Geoscience and Remote Sensing*, vol. 60, pp. 1–18, 2022.